A Mathematical Model of a Lithium/Thionyl Chloride Primary Cell

by

T. I. Evans*, T. V. Nguyen*, and R. E. White**

Department of Chemical Engineering

Texas A&M University

College Station, Texas 77843

$IN-33-CR$

213089

$5\ 1p.$

* Electrochemical Society Student Member

**Electrochemical Society Active Member

ABSTRACT

A one-dimensional mathematical model for the lithium/thionyl chloride primary cell has been developed to investigate methods of improving its performance and safety. The model includes many of the components of a typical lithium/thionyl chloride cell such as the porous lithium chloride film which forms on the lithium anode surface. The governing equations are formulated from fundamental conservation laws using porous electrode theory and concentrated solution theory. The model is used to predict one-dimensional, time dependent profiles of concentration, porosity, current, and potential as well as cell temperature and voltage. When a certain discharge rate is required, the model can be used to determine the design criteria and operating variables which yield high cell capacities. Model predictions can be used to establish operational and design limits within which the thermal runaway problem, inherent in these cells, can be avoided.

INTRODUCTION

The lithium/thionyl chloride (Li/SOCl$_2$) cell is an attractive primary energy source because of its high energy density (1, 2). However, researchers have observed that the Li/SOCl$_2$ cell is a serious safety hazard under certain conditions (2). High discharge rates and high temperatures promote thermal runaway which can result in the venting of toxic gases and explosion. A mathematical model of this battery has been developed to investigate the operational and design characteristics which can be adjusted to yield efficient, yet acceptably safe Li/SOCl$_2$ cells.

Description of Li/SOCl$_2$ cell

The model describes the Li/SOCl$_2$ cell illustrated in Fig. 1. The four cell regions are the lithium foil anode, the lithium chloride (LiCl) film which forms on the anode surface, the separator (usually a glass matting), and the porous carbon cathode. The anode surface and cathode current collector are the boundaries of the model region. The electrolyte consists of lithium tetrachloroaluminate (LiAlCl$_4$) in thionyl chloride (SOCl$_2$). The Li/SOCl$_2$ cell is a complex chemical and electrochemical system involving an unknown number of reactions (2). The overall reactions which seem most important to include in modeling are: the oxidation of lithium at the anode

$$Li \longrightarrow Li^+ + e^- \qquad [1]$$

the reduction of SOCl$_2$ at the cathode

$$2SOCl_2 + 4e^- \longrightarrow 4Cl^- + SO_2 + S \qquad [2]$$
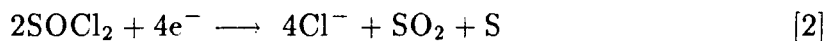
and the formation of the LiCl film on the anode and the precipitation of LiCl on the pore surfaces of the cathode during discharge by the following reaction

$$Li^+ + Cl^- \rightleftharpoons LiCl(s) \qquad [3]$$

1

Reaction [3] is assumed to occur completely and instantaneously, thus, reactions [2] and [3] can be combined to yield one overall reaction representing the processes occurring within the porous cathode

$$4Li^+ + 4e^- + 2SOCl_2 \longrightarrow 4LiCl + SO_2 + S \qquad [4]$$
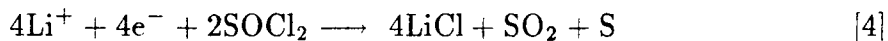
Four species are included in the model: Li^+, $AlCl_4^-$, $SOCl_2$, and LiCl. Since the chloride ion, Cl^-, does not appear in reaction [4] it is not included in the model. Later, this species may be included because of its influence on species transport (3). In addition, SO_2 and S are not included in the model because it is assumed that they dissolve into the electrolyte (4). These assumptions simplify the model development; the more species considered, the more complex and cumbersome the transport equations become. The species S and SO_2 may be included at a later time because researchers have shown that SO_2 is the major component in the vapor phase and that S precipitates with the LiCl in the porous cathode (5).

Szpak and Venkatsetty (6) state that modeling the $Li/SOCl_2$ cell is difficult due to the complexity of this physical system. They observe that as the cell discharges, the temperature and pressure of the cell change, the volume of electrolyte decreases, the electrolyte composition varies, and new phases appear. However, much can be learned from attempting to describe these phenomena through mathematical modeling.

Models of the $Li/SOCl_2$ cell

Previous workers have presented mathematical models of the $Li/SOCl_2$ cell (3, 7-14) as well as mathematical models of similar electrochemical systems (15-19). The $Li/SOCl_2$ cell model developed by Tsaur and Pollard (7) is based on conservation of mass and charge and is used to determine the concentration and

reaction rate profiles in the cell. Other Li/SOCl$_2$ cell models (10-14) are based on conservation of energy and are used to determine the thermal behavior of the cell.

Tsaur and Pollard (3, 7, 8) present a one-dimensional model of the Li/SOCl$_2$ cell. They use porous electrode theory (20, 21) and concentrated solution theory (22-24) to develop this model, and then use their model to predict concentration profiles, reaction rate distributions in the porous electrode, distributions of LiCl precipitate in the pores of the porous electrode, and cell utilization. However, in their model development Tsaur and Pollard (3, 7, 8) assume that the reservoir is a well mixed solution of constant concentration, which may not be a valid assumption as shown by Gu et al. (15). Also, they do not treat the LiCl film as a separate region in their model but end their calculations at the LiCl film/separator interface. This work shows the importance of including the film region in the modeling as evidenced by the large concentration gradients in the film and the effect of film porosity on cell performance.

Several models (10-14) have been presented to describe the thermal behavior of Li/SOCl$_2$ cells. Parnell and Szpak (10) present a thermal model for the Li/SOCl$_2$ cell in one dimension. They consider heat generation due to the polarization of the electrodes and internal cell resistance. Their model is used to show that as the rate of discharge is increased, the temperature increase is proportional to the increase in cell current. Szpak et al. (11) present a thermal model, similar to the model by Parnell and Szpak (10), which accounts for catastrophic thermal runaway. This model (11) is formulated based on the fact that thermal runaway is associated with ignition and burning, via one or more cell defects, rather than explosion. The model is used to predict the time and position dependent temperature and concentration profiles. The model predictions compare favorably to what is physically observed which may indicate that the reactions causing thermal runaway are initiated by localized heat sources developed from

3

defective cells and/or cell components. Cho and Halpert (12) have presented a simple thermal model for $Li/SOCl_2$ primary cells. Using experimental data for a specific cell discharge to determine a heat generation rate term, they use their model to predict the cell temperature as it changes with time. This information can be used to determine safe operating limits for a particular cell. Cho and Halpert (13) and Cho (14) have taken the modeling one step further by developing a means to calculate the heat generation rate term in their model (12) using experimentally determined resistances. These thermal models (10-14) are simple models which describe the cell using a small set of equations, unknowns, and parameters. These models are limited as far as their ability to predict cell behavior as a function of various design criteria because they do not include many features of the physical system. For example, the models do not include the effects of migration on species transport, the effect of the precipitating LiCl in the porous electrode on reaction kinetics, and the effects of current and potential on the electrochemical reaction rates. These models cannot be used to predict certain key design criteria, such as the porosity distribution in the porous cathode.

Models of similar electrochemical systems, such as the models of the lead acid battery (15-17) and the lithium-aluminum/iron sulfide battery (18, 19), were found to be useful in the development of the model presented here. These models, like Tsaur and Pollard's model (7), are based on conservation of mass and charge and employ concentrated solution theory as well as porous electrode theory. Some of the model equations here are similar to those presented in these models. Although similar, these models cannot be used to model the $Li/SOCl_2$ cell because they do not include all the various regions in the $Li/SOCl_2$ cell nor do they include certain physical phenomena specific to the $Li/SOCl_2$ cell, such as the LiCl film formed on the lithium anode surface.

MODEL DEVELOPMENT

The governing equations presented next describe conservation of mass and current, species transport, and reaction kinetics in each region of the $Li/SOCl_2$ cell. The equations for the porous electrode region are presented first, followed by the equations for the reservoir, separator, and LiCl film. The boundary conditions and initial conditions necessary to complete the equation set are presented next. The overall energy balance used to determine the cell temperature as it changes with time is presented last.

Porous electrode region

In order to develop a useful and descriptive set of governing equations for the porous electrode its essential features must be accounted for without considering its random microscopic geometry. The macroscopic theory for porous electrodes, introduced by Newman and Tiedemann (20) is used for this purpose. Essentially, the porous region is treated as a superposition of two continua, the ionically conducting electrolyte (solution) phase and the electronically conducting matrix (solid) phase. That is, the porous electrode is pictured as one homogeneous region which can be described by various distributed quantities. These quantities are continuous in space and time and are averaged over a differential volume of the porous region which is small relative to the overall dimensions of the electrode yet large relative to the pore structure. This volume averaging procedure has been used to model other electrochemical systems (15, 25) and is discussed in detail by Trainham (21), Whitaker (26), and Dunning (27). Examples of volume averaged quantities are the Faradaic current in the solution phase and the electronic current in the matrix phase of the porous electrode.

The current in the porous region must be conserved. Assuming that the double layer at the pore wall is extremely thin relative to the pore dimensions,

5

the electrolyte within the pores can be considered electrically neutral and governed by the electroneutrality condition which is

$$\sum_i z_i c_i = z_+ c_+ + z_- c_- = 0 \qquad [5]$$

Then, conservation of charge requires that the charge entering the solution phase, i_2, must be equal to the charge leaving the matrix phase, i_1, which in one dimension is expressed as follows

$$\frac{\partial i_{1,x}}{\partial x} + \frac{\partial i_{2,x}}{\partial x} = 0 \qquad [6]$$

The total current transferred from the matrix phase to the solution phase, $\partial i_{1,x}/\partial x$ or $\partial i_{2,x}/\partial x$, is equal to the net rate of electrochemical reaction per unit volume of electrode

$$j = a \sum_k i_k = \frac{\partial i_{2,x}}{\partial x} = -\frac{\partial i_{1,x}}{\partial x} \qquad [7]$$

where j is the local transfer current in A/cm^3 and i_k is the rate of electrochemical reaction k per unit area of active electrode surface area.

The material balance equation for each species i in the solution phase is,

$$\frac{\partial(\epsilon c_i)}{\partial t} = -\nabla \cdot \mathbf{N}_i + R_i \qquad (i = +, -, o) \qquad [8]$$

where,

$$R_i = -\sum_k \frac{s_{i,k} a}{n_k F} i_k \qquad [9]$$

The subscripts $+$, $-$, and o refer to Li^+, $AlCl_4^-$, and $SOCl_2$, respectively. In Eq. [8], ϵ represents the fraction of the porous electrode volume which is void of the matrix phase and filled with electrolyte, c_i is the concentration of species i in the solution, $\mathbf{N}_i$ is the flux of species i averaged over the cross sectional area of the porous region, and R_i is the production rate of species i per unit volume of electrode due to chemical or electrochemical reaction. Here, reaction [4] is assumed to be the only reaction occurring within the porous region.

Concentrated solution theory (22-24), in particular the multicomponent diffusion equation (MDE), is used to develop the equations describing the species transport. This theory is used because the solvent, $SOCl_2$, is involved in an electrochemical reaction and is not present in excess amounts relative to the solute, $LiAlCl_4$. The MDE for a given species can be thought of as a force balance which describes how the motion of that species is affected by the motion of all the other species in the electrolyte. The MDEs are inverted (22-24) to obtain explicit expressions for the species fluxes. The resulting flux expressions for a binary electrolyte are

$$\mathbf{N}_i = -D_{eff}\nabla c_i + \frac{i_2 t_i^{\blacksquare}}{z_i F} + c_i \mathbf{v}^{\blacksquare} \qquad (i = +, -) \qquad [10]$$

$$\mathbf{N}_o = -D_{eff}\nabla c_o + c_o \mathbf{v}^{\blacksquare} \qquad [11]$$

In Eq. [10] and [11] the volume average velocity is defined (28)

$$\mathbf{v}^{\blacksquare} = \sum_i \mathbf{N}_i \tilde{V}_i = \sum_i c_i \tilde{V}_i \mathbf{v}_i \qquad (i = +, -, o) \qquad [12]$$

and the effective diffusivity, D_{eff}, is defined

$$D_{eff} = D\epsilon^{expe} \qquad [13]$$

where $expe$ is chosen to be 1.5; this value is consistent with earlier work (7, 15). Eq. [13] relates the electrolyte diffusivity in the porous region, D_{eff}, to that in the bulk solution, D, by accounting for the effects of porosity and tortuosity in the porous region (7, 15).

Solvent and electrolyte material balances:

Equations [9], [10], [11], and [13] are introduced into Eq. [8] to obtain the following material balance expressions for the charged species and for the solvent

$$\frac{\partial(\epsilon c_i)}{\partial t} = -\nabla \cdot \left(-D\epsilon^{expe}\nabla c_i + \frac{i_2 t_i^{\blacksquare}}{z_i F} + c_i \mathbf{v}^{\blacksquare} \right) - \sum_k \frac{s_{i,k} a}{n_k F} i_k \qquad (i = +, -) \qquad [14]$$

7

$$\frac{\partial(\epsilon c_o)}{\partial t} = -\nabla \cdot \left(-D\epsilon^{expe}\nabla c_o + c_o\mathbf{v}^\blacksquare \right) - \sum_k \frac{s_{o,k}a}{n_k F}i_k \tag{15}$$

Equations [14], corresponding to the two unknowns c_+ and c_-, can be reduced to one equation for one unknown by introducing the following relationship

$$c = \frac{c_+}{\nu_+} = \frac{c_-}{\nu_-} \tag{16}$$

Equation [16] expresses conservation of mass for a completely dissociated salt, here LiAlCl$_4$, where c is the concentration of the salt (or electrolyte). In Eq. [16], ν_+ and ν_- are the number of Li$^+$ and AlCl$_4^-$ ions formed from the complete dissociation of one molecule of LiAlCl$_4$, respectively. Substituting Eq. [16] into Eq. [14] yields the electrolyte material balance

$$\frac{\partial(\epsilon c)}{\partial t} = -\nabla \cdot \left(-D\epsilon^{expe}\nabla c + \frac{\mathbf{i}_2 t_+^\blacksquare}{z_+\nu_+ F} + c\mathbf{v}^\blacksquare \right) - \sum_k \frac{s_{+,k}a}{n\nu_+ F}i_k \tag{17}$$

Note that either relation in Eq. [16] can be substituted into the corresponding species balance, Eq. [14], to obtain the same result, Eq. [17]. The cation ($i = +$) material balance was chosen here to derive Eq. [17].

Solid phases material balance:

Equation [8] for the solid phases, LiCl here, is

$$\frac{\partial \epsilon}{\partial t} = \sum_i^{\text{solid phases}} \sum_k \frac{s_{i,k}\bar{V_i}}{n_k F}ai_k \tag{18}$$

Equation [18] describes the porosity change of the porous cathode as LiCl precipitates in the pores.

Overall material balance:

The three material balance equations are: Eq. [15] for the solvent, Eq. [17] for the electrolyte, and Eq. [18] for the solid species. These equations contain the four

8

unknowns, c, c_o, ϵ, and $\mathbf{v}^\blacksquare$. The unknown c_o can be eliminated from these equations via the following independent thermodynamic relationship

$$1 = c\tilde{V}_e + c_o\tilde{V}_o \qquad [19]$$

where the partial molar volume of the electrolyte, $\tilde{V}_e$, is defined as

$$\tilde{V}_e = \nu_+\tilde{V}_+ + \nu_-\tilde{V}_- \qquad [20]$$

Equation [19] expresses conservation of volume and can be thought of as a definition for the partial molar volumes $\tilde{V}_i$ (29). When Eq. [14] and [15] are premultiplied by $\tilde{V}_+$, $\tilde{V}_-$, and $\tilde{V}_o$, respectively, and the three resulting equations are substituted into Eq. [18] an overall material balance is obtained. This is true because the resulting equation is a linear combination of all the species balances. Equation [19] is used to simplify this balance to yield the following overall material balance expression

$$\nabla \cdot \mathbf{v}^\blacksquare = -\sum_k \frac{1}{n_k F} \left[\sum_i^{\text{solid species}} s_{i,k}\tilde{V}_i + \left(\tilde{V}_o s_{o,k} + \tilde{V}_e t_-^\blacksquare s_{+,k} + \tilde{V}_e t_+^\blacksquare s_{-,k} \right) \right] \nabla \cdot \mathbf{i_2} \quad [21]$$

In one dimension, Eq. [21] can be integrated to yield an explicit expression for $v_x^\blacksquare$ in terms of $i_{2,x}$. Based on the fact that the current is zero when the velocity is zero,

$$v_x^\blacksquare = i_{2,x} = 0 \qquad [22]$$

integration of Eq. [21] yields

$$v_x^\blacksquare = -\sum_k \frac{1}{n_k F} \left[\sum_i^{\text{solid species}} s_{i,k}\tilde{V}_i + \left(\tilde{V}_o s_{o,k} + \tilde{V}_e t_-^\blacksquare s_{+,k} + \tilde{V}_e t_+^\blacksquare s_{-,k} \right) \right] i_{2,x} \quad [23]$$

9

Ohm's law for the electrolyte:

The Faradaic current density, i_2, is a function of the chemical potential, μ_e, and solution potential, Φ_2 (20, 24). This relationship, Ohm's law for the solution phase, for a binary electrolyte is (24)

$$\frac{i_2}{\kappa_{eff}} = -\nabla\Phi_2 - \frac{\nu RT}{F}\left(\frac{s_{+,4}}{n_4\nu_+} + \frac{t_+^{\blacksquare}}{z_+\nu_+} - \frac{s_{o,4}c}{n_4 c_o}\right)\nabla\mu_e \qquad [24]$$

where

$$\nu = \nu_+ + \nu_- \qquad [25]$$

and

$$\mu_e = \nu_+\mu_+ + \nu_-\mu_- = \nu RT \ln(cfa^\theta) \qquad [26]$$

In Eq. [24] the effective electrolyte conductivity, κ_{eff}, is defined analogously to the effective electrolyte diffusivity, D_{eff}.

$$\kappa_{eff} = \kappa\epsilon^{expe} \qquad [27]$$

Equations [19], [26], and [27] can be substituted into Eq. [24] to yield the following Ohm's law expression for the electrolyte

$$\frac{i_2}{\kappa\epsilon^{expe}} = -\nabla\Phi_2 - \frac{\nu RT}{F}\left(\frac{s_{+,4}}{n_4\nu_+} + \frac{t_+^{\blacksquare}}{z_+\nu_+} - \frac{s_{o,4}c\tilde{V}_o}{n_4(1 - c\tilde{V}_e)}\right)\frac{\nabla c}{c} \qquad [28]$$

Ohm's law for the matrix phase:

Ohm's law for the matrix phase is (15, 20)

$$i_1 = -\sigma_{eff}\nabla\Phi_1 \qquad [29]$$

where

$$\sigma_{eff} = \sigma(1 - \epsilon^o)^{expe} \qquad [30]$$

Equation [30] is used to account for the effect of the matrix phase tortuosity on the conductivity of the solid material, σ. The initial porosity, ϵ^o, is used in Eq. [30] because the matrix conductivity is assumed to change insignificantly as LiCl precipitates.

Equation [6] can be used to eliminate i_1 from Eq. [29]. Integrating Eq. [6] with respect to x and applying the boundary conditions

$$\text{at } x = 0, \qquad i_{1,x} = I \quad \text{and} \quad i_{2,x} = 0 \qquad [31]$$

results in the following relationship

$$i_{1,x} + i_{2,x} = I \qquad [32]$$

Substituting Eq. [32] into Eq. [29] yields

$$I - i_{2,x} = -\sigma_{eff}\frac{\partial \Phi_1}{\partial x} \qquad [33]$$

Electrode kinetics:

The electrochemical reaction rates, i_k, in Eq. [17] and [18] depend upon the local concentrations of the chemical species, the potential driving force for reaction, and temperature. Analogous to chemical kinetics, these dependencies are not described by fundamental laws. The Butler-Volmer polarization equation (15, 30) is used here

$$i_k = i_{o,k,ref}\left[\prod_i\left(\frac{c_i}{c_{i,ref}}\right)^{p_{i,k}} \exp\left(\frac{\alpha_{a,k}F}{RT}(\Phi_1 - \Phi_2 - U_{k,ref})\right)\right.$$

$$\left. - \prod_i\left(\frac{c_i}{c_{i,ref}}\right)^{q_{i,k}} \exp\left(-\frac{\alpha_{c,k}F}{RT}(\Phi_1 - \Phi_2 - U_{k,ref})\right)\right] \qquad [34]$$

The potential driving force for electrochemical reaction k is $\Phi_1 - \Phi_2 - U_{k,ref}$ where $U_{k,ref}$ is the equilibrium potential of reaction k measured relative to the

reference electrode. The electro-kinetic parameters $i_{o,k,ref}$, $\alpha_{a,k}$, and $\alpha_{c,k}$ are the exchange current density, anodic transfer coefficient, and cathodic transfer coefficient, respectively. The transfer coefficients for a given reaction sum to the total number of electrons involved in that reaction

$$\alpha_{a,k} + \alpha_{c,k} = n_k \qquad [35]$$

The rate of reaction k per unit volume of porous electrode is ai_k where a is the available active surface area per unit volume of electrode. The variable a changes as the LiCl precipitates on the pore walls, according to reaction [4], and can be described by (27, 31)

$$a = a^o\left[1 - \left(\frac{\epsilon^o - \epsilon}{\epsilon^o}\right)^{mp}\right] \qquad [36]$$

where mp is an experimentally determined parameter used to describe the morphology of the precipitate. In writing Eq. [36] it is assumed that all the LiCl produced from reaction [4] precipitates instantaneously and passivates the surface it covers. Large values of mp indicate needle-shaped deposits whereas small values represent flat deposits (31).

Substituting Eq. [34] and [36] into Eq. [7] yields the following equation expressing conservation of current

$$\frac{\partial i_{2,x}}{\partial x} = a^o\left[1 - \left(\frac{\epsilon^o - \epsilon}{\epsilon^o}\right)^{mp}\right]\sum_k i_{o,k,ref}\left[\prod_i\left(\frac{c_i}{c_{i,ref}}\right)^{p_{i,k}}\exp\left(\frac{\alpha_{a,k}F}{RT}\right.\right.$$

$$\left.\left.(\Phi_1 - \Phi_2 - U_{k,ref})\right) - \prod_i\left(\frac{c_i}{c_{i,ref}}\right)^{q_{i,k}}\exp\left(-\frac{\alpha_{c,k}F}{RT}(\Phi_1 - \Phi_2 - U_{k,ref})\right)\right] \qquad [37]$$

Altogether, six equations and six unknowns are used to describe the porous electrode region. The six equations are the electrolyte material balance, Eq. [17]; the solid species material balance, Eq. [18]; the overall material balance, Eq. [23]; Ohm's law for the electrolyte, Eq. [28]; Ohm's law for the matrix phase, Eq. [33];

12

and conservation of current using the Butler-Volmer equation, Eq. [37]. The six unknowns are the electrolyte concentration, c; the porosity, ϵ; the volume average velocity, $v_x^{\blacksquare}$; the Faradaic current density, $i_{2,x}$; the potential in the matrix phase, Φ_1: and the potential in the solution phase, Φ_2. Simplified forms of Eq. [17], [18], [23], [28], [33] and [37] are used to describe the remaining regions of the cell: the reservoir, the separator, and the LiCl film.

Reservoir

The reservoir, the space between the separator and the positive porous electrode, contains electrolyte and serves to supply $SOCl_2$ to the positive electrode as it is consumed via reaction [4]. The solid matrix phase does not exist in this region, therefore the unknowns ϵ, $i_{1,x}$, and Φ_1 have no meaning. They are treated as dummy variables and their values are arbitrarily set as follows

$$\epsilon = 1 \tag{38}$$

$$\Phi_1 = 0 \tag{39}$$

$$i_{1,x} = 0 \tag{40}$$

Using Eq. [40] in Eq. [32] yields

$$i_{2,x} = I \tag{41}$$

Equations [17] and [28] for the porous electrode can be simplified for the reservoir using Eq. [38] and [41]. The electrolyte balance becomes

$$\frac{\partial c}{\partial t} = D \nabla^2 c - \nabla \cdot (c \mathbf{v}^{\blacksquare}) \tag{42}$$

and Ohm's law for the electrolyte becomes

$$\frac{I}{\kappa} = -\nabla \Phi_2 - \frac{\nu RT}{F} \left(\frac{s_{+,4}}{n_4 \nu_+} + \frac{t_+^{\blacksquare}}{z_+ \nu_+} - \frac{s_{o,4} c \bar{V}_o}{n_4 (1 - c \bar{V}_e)} \right) \frac{\nabla c}{c} \tag{43}$$

Note that effective properties are not used in Eq. [42] and [43] because no matrix phase exists. Equation [23] is used to calculate the volume average velocity. In summary, the six governing equations for this region are Eq. [23], [38], [39], [41], [42], and [43].

Separator

The separator is an inert, porous layer (usually a glass matting material) which prevents the negative and positive electrodes from touching and thus shorting the cell. The separator porosity (ϵ_s) is constant, hence

$$\epsilon = \epsilon_s \qquad [44]$$

The solid phase of the separator is a non-conducting material; Φ_1 does not exist and is set to zero as in Eq. [39]. All current resides in the electrolyte, hence Eq. [41] applies. Using Eq. [41] and [44] to simplify Eq. [17] and [28], the electrolyte balance for the separator is

$$\epsilon_s \frac{\partial c}{\partial t} = D\epsilon_s^{exs} \nabla^2 c - \nabla \cdot (c\mathbf{v}^\blacksquare) \qquad [45]$$

and Ohm's law for the electrolyte is

$$\frac{I}{\kappa \epsilon_s^{exs}} = -\nabla \Phi_2 - \frac{\nu RT}{F} \left(\frac{s_{+,4}}{n_4 \nu_+} + \frac{t_+^\blacksquare}{z_+ \nu_+} - \frac{s_{o,4} c \tilde{V}_o}{n_4 (1 - c\tilde{V}_e)} \right) \frac{\nabla c}{c} \qquad [46]$$

Note that effective properties have been used in Eq. [45] and [46] to characterize the transport and conductivity in the separator. The exponent *exs* is analogous to *expe* and its value is set to 1.5. The overall material balance is Eq. [23]. In summary, the six governing equations for the separator are Eq. [23], [39], [41], [44], [45], and [46].

Lithium chloride film

14

The stability of the lithium anode is attributed to the LiCl film which forms from the corrosion of the Li by the $SOCl_2$ on open circuit (32-35)

$$4Li + 2SOCl_2 \longrightarrow 4LiCl + SO_2 + S \qquad [47]$$
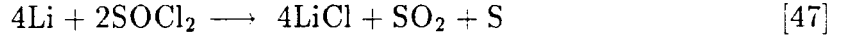
Researchers (32-35) believe that the film passivates the Li and inhibits the mass transport of $SOCl_2$ to the Li surface. Some workers (34, 35) have described the LiCl film as consisting of two parts: a relatively thin, non-porous layer of LiCl formed on top of the Li anode surface called the solid electrolyte interphase (SEI) and a much thicker, porous layer of LiCl formed on top of the SEI called the secondary porous layer. These workers have proposed that it is the SEI which passivates the Li surface because the secondary layer has a coarse crystalline, porous structure (32) which cannot be assumed to have the resistance properties necessary for complete passivation of the Li. Peled (35) views the secondary porous layer as a membrane which inhibits the flow of ions to and from the SEI. Here, the transition between the SEI and secondary layer is assumed to be distinct, and the layers are treated separately. The SEI surface is treated here as the Li anode surface having modified (passivation) kinetics and the secondary porous LiCl layer is treated here like a separator.

The governing equations for the secondary, porous LiCl film are developed in the same manner as those for the separator. The equations are: a constant porosity

$$\epsilon = \epsilon_f \qquad [48]$$

the electrolyte balance,

$$\epsilon_f \frac{\partial c}{\partial t} = D\epsilon_f^{exf} \nabla^2 c - \nabla \cdot (c\mathbf{v}^\blacksquare) \qquad [49]$$

Ohm's law for the electrolyte,

$$\frac{I}{\kappa \epsilon_f^{exf}} = -\nabla \Phi_2 - \frac{\nu RT}{F} \left(\frac{s_{+,4}}{n_4 \nu_+} + \frac{t_+^\blacksquare}{z_+ \nu_+} - \frac{s_{o,4} c \bar{V}_o}{n_4 (1 - c\bar{V}_e)} \right) \frac{\nabla c}{c} \qquad [50]$$

15

and Eq. [23], [39], [41]. The value of the exponent exf is set to 1.5.

The secondary porous film grows as time progresses but its thickness is kept constant here. Film growth may occur by reaction [3] where the Cl^- ions are a product of the cathode reaction. Tsaur and Pollard (7) assume that the rate of reaction [47] governs the film growth. However, reaction [47] is the sum of the two electrochemical half reactions [1] and [4] and does not occur on discharge because the lithium is anodically protected. The secondary porous layer is not of uniform thickness over the surface of the lithium (33), its morphology depends strongly on the storage temperature (33), and mechanical rupture may occur during discharge (32). Because of these complications, the film thickness is kept constant and can be thought of as an average value of the thickness which varies in space and time. The model will be used to predict the effects of the film thickness and porosity on the cell performance.

Boundary conditions

The boundaries, from left to right in Fig. 1, are the Li anode surface (taken as the SEI surface here), the LiCl film/separator interface, the separator/reservoir interface, the reservoir/porous cathode interface, and the cathode current collector surface. The governing equations at each boundary are given next.

SEI surface:

The SEI is treated as the Li anode surface with modified kinetics. The rate of reaction [1] is calculated using Eq. [34] with kinetic parameters representing the passivation. Lithium ions must travel from the SEI surface at the same rate at which they are produced, thus the flux of this species must equal its reaction rate

$$\mathbf{N}_+ = -\nu_+ D \epsilon_f^{exf} \nabla c|_f + \frac{i_2 t_+^{\bullet}}{z_+ F} + \nu_+ c \mathbf{v}^{\bullet} = -\frac{s_{+,1}}{n_1 F} i_1 \qquad [51]$$

The solvent flux is zero at this boundary

$$\mathbf{N}_o = -D\epsilon_f^{ex f}\nabla c_o|_f + c_o\mathbf{v}^\blacksquare = 0 \tag{52}$$

Using Eq. [19], Eq. [52] can be written

$$\mathbf{N}_o = D\epsilon_f^{ex f}\tilde{V}_e\nabla c|_f + (1 - c\tilde{V}_e)\mathbf{v}^\blacksquare = 0 \tag{53}$$

In Eq. [51] - [53], and in equations to follow, the vertical bar and subscript, $|_y$, indicate that the preceding quantity is evaluated at the interface of the region y. At the film interface, all the current is transferred from the anode surface to the solution phase, hence $i_{1,x}$ is zero and Eq. [41] applies. Equation [7] for a flat plate electrode is

$$I = \sum_k i_k \tag{54}$$

where Eq. [34] is used to calculate i_k. The porosity is treated as a dummy variable and it is arbitrarily set equal to the LiCl film porosity, Eq. [48]. At this boundary Φ_1 is arbitrarily set to zero, Eq. [39], to establish a reference point from which to calculate all other potentials. The absolute values of Φ_1 and Φ_2 have no significance; only the value of the difference $\Phi_1 - \Phi_2$ is meaningful. The value of Φ_2, given Eq. [39], is determined from Eq. [54]. In summary, the boundary conditions at the SEI boundary are Eq. [39], [41], [48], [51], [53], and [54].

LiCl film/separator interface:

At this boundary the flux of each species i is continuous

$$\mathbf{N}_i\big|_f = \mathbf{N}_i\big|_s \tag{55}$$

and the velocity is continuous

$$v_x^\blacksquare\big|_f = v_x^\blacksquare\big|_s \tag{56}$$

17

Substituting Eq. [10], [16], [19], and [56] into Eq. [55] yields the following equation expressing continuity of the electrolyte flux

$$\epsilon_f^{exf} \nabla c \big|_f = \epsilon_s^{exs} \nabla c \big|_s \qquad [57]$$

Equation [46] for the separator and Eq. [50] for the LiCl film are equated, and Eq. [57] is used, to yield the following equation which expresses continuity of Faradaic current

$$\epsilon_f^{exf} \nabla \Phi_2 \big|_f = \epsilon_s^{exs} \nabla \Phi_2 \big|_s \qquad [58]$$

As in the film and separator regions, Eq. [39] and [41] apply. The porosity is arbitrarily set equal to ϵ_s, Eq. [44]. In summary, the boundary conditions at this boundary are Eq. [39], [41], [44], [56], [57], and [58].

Separator/reservoir interface:

The boundary conditions here are analogous to those at the LiCl film/separator boundary. These equations are: continuity of flux

$$\epsilon_s^{exs} \nabla c \big|_s = \nabla c \big|_r \qquad [59]$$

continuous velocity

$$v_x^{\blacksquare} \big|_s = v_x^{\blacksquare} \big|_r \qquad [60]$$

continuity of Faradaic current

$$\epsilon_s^{exs} \nabla \Phi_2 \big|_s = \nabla \Phi_2 \big|_r \qquad [61]$$

and Eq. [39], [41], and [44].

Reservoir/porous electrode interface:

The boundary conditions at this interface include continuity of flux

$$\nabla c \big|_r = \epsilon^{expe} \nabla c \big|_{pe} \qquad [62]$$

18

continuity of Faradaic current

$$\nabla\Phi_2\big|_r = \epsilon^{expe}\nabla\Phi_2\big|_{pe} \qquad [63]$$

and Eq. [41]. This boundary includes the porous electrode surface, hence porosity will change as will the volume average velocity as described by Eq. [18] and [23], respectively. Equation [33] is applied at this boundary as follows

$$\nabla\Phi_1\big|_{pe} = 0 \qquad [64]$$

Porous electrode current collector surface:

A Li/SOCl$_2$ battery may be pictured in one dimension as a series of cells sandwiched together. The current collector of the porous cathode separates the cathodes of two consecutive cells. With this configuration in mind, the one dimensional distribution of the Faradaic current density will be essentially zero at the current collector. That is, it is assumed that all of the current has been transferred from the solution phase to the matrix phase at the current collector, thus

$$i_{2,x} = 0 \qquad [65]$$

Also, the volume average velocity is assumed to be essentially zero at this boundary

$$v_x^\blacksquare = 0 \qquad [66]$$

As at the SEI surface, the flux of the each species must equal its reaction rate. The electrolyte flux is zero here

$$\mathbf{N}_+ = -\nu_+ D\epsilon^{expe}\nabla c\big|_{pe} + \frac{i_2 t_+^\blacksquare}{z_+ F} + \nu_+ c v^\blacksquare = 0 \qquad [67]$$

Using Eq. [65] and [66], Eq. [67] can be written

$$\nabla c\big|_{pe} = 0 \qquad [68]$$

19

Similarly, Eq. [28] becomes

$$\nabla \Phi_2|_{pe} = 0 \qquad [69]$$

The transfer current at this boundary is given by

$$\left. \frac{\partial i_{2,x}}{\partial x} \right|_{pe} = j \qquad [70]$$

where j is calculated using Eq. [7], [34], and [36]. The porosity change is calculated using Eq. [18].

Initial conditions

To complete the equation set, the initial conditions must be specified for those variables that depend explicitly on time, c and ϵ. These initial conditions are

$$c = c_{init} \qquad \text{(all x)} \qquad [71]$$

$$\epsilon = \epsilon^o \qquad \text{(porous electrode)} \qquad [72]$$

Cell energy balance

An energy balance is included in the model to determine the cell temperature as it changes with time. The energy balance follows from the first law of thermodynamics

$$\frac{du}{dt} = \frac{dq}{dt} + \frac{dw}{dt} \qquad [73]$$

where u is the internal energy of the cell. When constant volume conditions are assumed

$$\frac{du}{dt} = C \frac{dT}{dt} \qquad [74]$$

The change in the work, dw/dt, is zero; no work is done on or by the cell when volume is constant. The change in the heat content of cell, dq/dt, is attributed to three sources (sinks): heat transferred across the cell boundaries ($\dot{q}_{ht}$), heat

generated by polarization ($\dot{q}_p$), and heat generated by entropy effects ($\dot{q}_s$) (36). The heat transfer can be described by

$$\dot{q}_{ht} = -h_o(T - T_A) \qquad [75]$$

where h_o is the heat transfer coefficient characterizing the heat flow from the cell to the surroundings. Here, the temperature of the surroundings is assumed to remain constant at T_A. The remaining two sources of heat are given by (36)

$$\dot{q}_p + \dot{q}_s = I\left(E_{oc} - E - T\frac{dE}{dT}\right) = I(E_{tn} - E) \qquad [76]$$

E_{tn} in Eq. [76], termed the thermoneutral potential, is the theoretical open circuit potential of the cell at absolute zero. Substituting Eq. [74], [75], and [76] into Eq. [73] yields the overall energy balance

$$C\frac{dT}{dt} = -h_o(T - T_A) + I(E_{tn} - E) \qquad [77]$$

Note that each term in Eq. [77] is based on the total active surface area in the cell. The initial condition for T here is

$$T = T_A \qquad \text{(all x)} \qquad [78]$$

21

MODEL PARAMETERS

The parameter values input to the model are listed in Table I. The partial molar volumes and transference numbers were assumed to be constant throughout the discharge at the values listed in Table I. The kinetic parameters $i_{o,1,ref}$, $\alpha_{a,1}$, $\alpha_{c,1}$, and $a^o i_{o,4,ref}$ were chosen so that the model predictions compared favorably with experimental data (32, 37-41). A temperature dependent expression for the diffusion coefficient and a temperature, concentration dependent expression for the conductivity are given in the appendix.

The independent adjustable parameters in this model development are the porous electrode thickness (S_{pe}), the initial porosity of the porous electrode (ϵ^o), the thickness of the electrolyte reservoir (S_r), the thickness of the separator (S_s), the porosity of the separator (ϵ_s), the LiCl film thickness (S_f), the LiCl film porosity (ϵ_f), the initial electrolyte concentration (c_{init}), the heat transfer coefficient (h_o), the current density (I), and the temperature of the surroundings (T_A). One objective of this work is to use the model to determine which of these independent adjustable parameters affects cell performance the most. Table II lists typical values for these independent adjustable parameters (5). Unless otherwise noted, these base case values are used throughout the work presented here.

METHOD OF SOLUTION

The system of coupled, nonlinear, ordinary differential equations describing the Li/SOCl$_2$ cell, shown in Fig. 1, is solved numerically because an analytical solution is not possible. The spatial derivatives are approximated using finite differences accurate to $O(\triangle x)^2$ where $\triangle x$ is the largest step size in the x direction. Implicit stepping, accurate to $O(\triangle t)$, is used for the time derivatives. A Newton-Raphson algorithm using deBoor's banded matrix solver (42-44) is used to solve the system of finite difference equations. The procedure is iterative and requires initial guesses of the unknowns. Step sizes in both space and time were reduced until predicted cell voltages were reproducible to three significant digits.

RESULTS AND DISCUSSION

Figure 2 shows predicted electrolyte concentration profiles and how they change with time. Note that the concentration profiles are relatively flat in the separator and reservoir regions indicating that diffusion, migration, and convection of species are essentially uninhibited in these regions. Convection contributes least to the species transport; $v_x^\blacksquare$ is $O(10^{-5})$ and the convection term is an order of magnitude less than the diffusion and migration terms in Eq. [17], [42], [45], and [49]. The large concentration gradients in the film region are due the small porosity of this region which reduces significantly the effective diffusivity. Near the beginning of discharge transport in the porous electrode region is essentially uninhibited. As the discharge proceeds, LiCl begins to fill the pores of the electrode and transport becomes more difficult as evidenced by the steeper concentration gradients at later times. The electrolyte concentration increases throughout the cell as time progresses and the solvent concentration decreases according to Eq. [19]. These profiles show that throughout most of the discharge cell performance is dictated by the rate of reaction [4] at the cathode. Tsaur and Pollard (7) predict diffusion control as evidenced by the large concentration gradients in the separator of their simulated cell; they assume a constant reservoir concentration *a priori*. This difference, reaction control here versus diffusion control (7), could be due to the different governing equations and boundary conditions as well as the differing input parameters used in their model and the present model. From Fig. 2 it can be seen that the change in the concentration across the reservoir is about half what it is in the separator and, under conditions of diffusion control, this change could effect results significantly. Higher discharge rates, lower temperatures, faster porous electrode reaction kinetics (i.e., larger exchange current densities for the thionyl chloride reduction on the carbon electrode), lower initial concentrations,

and smaller porosities all contribute to changing the reaction controlled conditions observed here to diffusion controlled conditions.

Figures 3-5 illustrate the space-time behavior of the porous electrode porosity, Faradaic current density, and overpotential, respectively. These profiles show that the reaction rate distribution changes very little as time progresses. The reaction rate will be greatest at the front of the porous electrode because the matrix conductivity (σ) is much larger than the electrolyte conductivity (κ) (7). That is, at the reservoir/porous electrode interface all current resides in the solution phase but upon entering the porous electrode the current will be transferred rapidly to the matrix phase because the matrix phase offers less resistance to current flow. However as LiCl precipitates, fills the pores as shown in Fig. 3, and decreases the available active surface area, according to Eq. [36], the reaction rate distribution becomes more uniform. This change can be seen in Fig. 4 where the $i_{2,x}$ distribution flattens out; the reaction rate is the slope if the $i_{2,x}$ versus x curve. Figure 5 shows that the overpotential, the driving force for electrochemical reaction, is highest at the front of the electrode as expected. The overpotential increases with time indicating that the electrochemical reaction must proceed at a faster rate to compensate for decreasing available active surface area.

As the end of discharge is approached the front portion of the electrode becomes clogged with LiCl precipitate (see Fig. 3). Lithium ions are unable to cross this barrier hence the electrolyte concentration increases rapidly in the film, separator, and reservoir as it is continually produced at the anode. At this point the electrolyte contained in the pores of the porous electrode supplies the lithium ions consumed in reduction reaction [4]. The electrolyte concentration drops in the vicinity of the highest reaction rate (the front of the electrode) and the electrolyte supply contained in the back portion of the electrode must diffuse to this reaction plane. This behavior can be seen from Fig. 4 where the current density distribution at $t =$

2160 seconds falls back from the flatter profiles exhibit at earlier times. Eventually, the front of the electrode becomes depleted of electrolyte and is unable to support further reaction, hence current flow, and the cell fails. This failure is indicated by the model when convergence cannot be achieved.

The model can be used to demonstrate the effects of the independent design criteria on cell performance. The least influential parameters, for the reaction controlled conditions here, were found to be S_r and S_s. For example, decreasing either S_r or S_s by an order of magnitude resulted in changes in the discharge time and cell voltage of less than 1%. The most influential parameters on cell performance were found to be S_{pe}, ϵ^o, and c_{init}. The parameters characterizing the LiCl film, ϵ_f and S_f, show small to moderate effects on cell performance.

As shown in Fig. 6, beyond a porous electrode thickness of approximately 0.1 cm there is little gain in cell lifetime. Apparently, for thicknesses beyond 0.1 cm the advantages of increased active surface area and electrolyte storage are diminished by the increase in cell resistance and hence decrease in cell lifetime. It is difficult to determine the effect of the porous electrode porosity on cell performance because when porosity is changed the active surface area, a, is also changed. Keeping a constant here, the cell lifetime is decreased by 49% and 86% for ϵ^o decreased to 0.6 and 0.35, respectively. This decrease in lifetime occurs simply because there exists less void volume for the precipitating LiCl to fill. Changes in S_{pe} and ϵ^o have very little effect on the operating voltage and temperature; the voltage and temperature varied by less than 1% for the cases studied here.

Figure 7 shows the predicted effect of initial electrolyte concentration on cell lifetime. Caution is needed when comparing cell performance for different concentrations because the average operating voltage decreases as initial electrolyte concentration decreases. For example, the average operating voltage for $c_{init} = 0.25$ M was about 8% lower than that for the base case. This concentration could

not be included in Fig. 7 because the predicted voltage transient fell below the cutoff voltage (2.9 V) chosen to determine cell lifetime. Beyond a concentration of approximately 2 M there is little increase in cell lifetime or average cell voltage. At concentrations below 1 M the overpotential required to drive the electrochemical reaction at a fast enough rate to support the current draw is necessarily high, especially at the front of the porous electrode. This acceleration of reaction rate causes the pores to fill up quickly with LiCl, and the cell fails rapidly as shown in Fig. 7. Also, for initial concentrations of about 0.5 M and below the shape of the cell voltage transient changes: cell voltage initially increases, reaches a maximum, and then decreases. This initial increase in voltage is attributed to the rather large initial increase in conductivity as the concentration of lithium ions increases as they are produced at the anode. Later the voltage decreases due to the decreasing porosity in the porous electrode and the resulting increase in resistivity.

The porosity of the LiCl film which forms on the lithium anode has a small effect on cell performance. Porosity of this film varies depending on storage temperature; higher storage temperatures tend to produce larger LiCl crystals and more compact films (33). Several observations can be made here from the model predictions. Film porosities beyond 0.1 seem to have little to no effect on cell lifetime, voltage, or temperature. Below a porosity of 0.1, cell voltage begins to decrease due to the greater hindrance of species transport in the film. For example, for a porosity of 0.05, the average cell voltage and cell lifetime are reduced by 3% as compared to the base case. When porosity is extremely low (e.g., 0.005) the model predicts that the cell will not operate for the 30 mA/cm^2 drain considered here. For a film porosity of 0.025, the model predicts higher cell temperatures (about 10°C higher on the average) and an average cell voltage about 11% lower than that for the base because of the increased cell resistance. These results show that it is advantageous

to maintain low temperature storage (room temperature) so that the film does not become too compact.

The film thickness has little effect on cell performance for the conditions studied here. Changes in cell lifetime of less than 0.1% are predicted when S_f is decreased to 0.5 microns or increased to 40 microns. However, depending on the film porosity, the average cell voltage can be decreased significantly when the film is thick. For the 40 micron film thickness, the average cell voltage was decreased by about 4% as compared to the base case.

The effect of discharge rate on cell voltage and temperature is shown in Fig. 8 and 9. Figure 8 shows the expected behavior of increased average cell voltage, lifetime, and capacity with decreased discharge rate. These curves compare favorably with experimental voltage-time curves (37, 38, 41). It is difficult to make detailed comparisons of model predictions with the experimental data reported in the literature due to the lack of cell specifications given (e.g., porous electrode porosity and thickness, and separator porosity and thickness). The temperature-time curves for various discharge rates are shown in Fig. 9. The initial rise in temperature is due to the polarization of the electrodes and entropy effects as represented by the terms $\dot{q}_p$ and $\dot{q}_s$ in Eq. [76]. As the temperature of the cell increases the rate of heat transfer to the surroundings increases until an equilibrium is almost reached where the heat transfer almost equals the heat generation. These equilibriums are represented by the plateaus in the curves in Fig. 9. At higher discharge rates these plateau become less distinct because the heat transfer cannot keep pace with the greater heat generation produced by the more severe electrode polarizations at higher discharge rates. At the end of discharge localized reactant depletion causes severe polarization and the cell temperature is driven upward at a faster rate as shown by the tail ends of the curves in Fig. 9. This surge in cell temperature at the end of discharge could lead to unsafe behavior by rapidly

increasing the internal pressure or possibly triggering exothermic runaway reactions (11). To avoid this hazard the cell could be operated below certain discharge rates and ambient temperature limits or it could be used up to a limited time well before reaching the end of discharge. These temperature profiles exhibit the same general pattern of experimental temperature-time curves (39). Improved heat transfer paths could be investigated using the model by changing the energy balance parameters, C and h_o, or modifying the energy balance, Eq. [77].

Model predictions are only as good as the input to the model. The results presented here are in good agreement with experimental data reported in the literature perhaps because of the detailed theoretical development and the trial and error perturbation of some of the kinetic parameters mentioned earlier. The kinetic parameters and physical properties used in the present analysis may change significantly for different applications which, in turn, could significantly effect model predictions. The versatility to change model inputs to simulate different applications is an important aspect of this model.

The kinetic parameters, $i_{o,1,ref}$, $a^o i_{o,4,ref}$, $\alpha_{a,1}$, $\alpha_{c,1}$, $\alpha_{a,4}$, $\alpha_{c,4}$, and the morphology parameter mp which is used to calculate a, are the least known because these parameters cannot be determined easily by experiment. Also these parameters are not constant values; the kinetic parameters for the $SOCl_2$ reduction are specific to the type of carbons used for the porous electrode, for example. The morphology parameter will change depending on the discharge rate and cell temperature. Experimental data along with complete cell specifications (including porosities) and physical property data (such as diffusivity and conductivity) could be used in conjunction with a parameter estimation technique to estimate these kinetic parameters. A detailed sensitivity analysis of the model predictions to changes in these kinetic parameters is beyond the scope of this work though a few items are of note. The oxidation exchange current density, $i_{o,1,ref}$, can significantly effect

29

cell voltage and lifetime whereas the reduction exchange current density, $a^o i_{o,4,ref}$, seems to influence cell lifetime more than cell voltage. For example, increasing $a^o i_{o,4,ref}$ by an order of magnitude results in a 15% reduction in cell life and a less than 1% increase in cell voltage.

Some of the physical properties used here were estimated from the available data in the literature (6, 7, 37, 45-47). An approximate expression for diffusivity, as described in the appendix, was used and constant transference numbers were assumed. The sensitivity of model predictions to small changes in these properties was briefly investigated. If D is halved, cell lifetime decreases by only 6%. If $t_+^\blacksquare$ is decreased to 0.25 there is an 18% decrease in cell lifetime due to the resulting decrease in species transport, Eq. [10], and the increase in IR drop across the cell as indicated by Ohm's law for the electrolyte. Changes in D and $t_+^\blacksquare$ have negligible effect on cell voltage and temperature. Similarly, changes in conductivity will directly effect the IR drop across the cell as dictated by the Ohm's law expression for the electrolyte. Decreasing conductivity will increase the IR drop and decrease cell voltage and lifetime.

CONCLUSIONS AND RECOMMENDATIONS

A one-dimensional model of a complete $Li/SOCl_2$ cell has been developed and used to demonstrate both design and operational changes that can be made to increase cell capacity and life. An unending number of cases could be studied using the model to determine optimal and safe designs for various cell specifications and discharge rates. This ability to investigate different designs simply by changing model inputs is where the value of the model lies. In addition, the model can be used along with a parameter estimation technique to estimate kinetic parameters for various carbon materials and electrolyte chemistries.

Improvements in the model would include accounting for the growth of the LiCl film as the cell discharges, the addition of the Cl^-, SO_2, and S species to determine their effects on cell performance, changing the energy balance to account for more complex heat transfer paths, and the modelling of a stack of cells representing the cross section of an entire $Li/SOCl_2$ battery. Also porous electrode swelling has been shown to be an important aspect of cell performance during high rate discharge (48) and should be added to the model.

ACKNOWLEDGEMENTS

APPENDIX: PHYSICAL PROPERTIES

The conductivity of the electrolyte, κ, is a function of concentration and temperature. Szpak and Venkatasetty (2) suggest that this functionality should be included in the battery modelling because of the large changes in the conductivity as the battery discharges. An empirical expression, similar in form to other conductivity expressions (7, 15, 16), describing this functionality has been developed from the available data (6, 37, 45-47)

$$\kappa = \begin{cases} \beta_1 c \exp(\beta_2 c + \beta_3 c^2) \exp(\beta_4/T) & (c < 1.8\ M) \\ \beta_5 \exp(\beta_4/T) & (c \geq 1.8\ M) \end{cases} \qquad [79]$$

where $\beta_1 = 135.45\ \Omega^{-1} cm^{-1}$, $\beta_2 = 399.09\ cm^3/mol$, $\beta_3 = $ -2.5055 $\times 10^{-5}\ cm^6/mol^2$, $\beta_4 = $ -711.69 K, and $\beta_5 = 0.22244\ \Omega^{-1} cm^{-1}$. The data for LiAlCl$_4$ mixtures (equimolar mixtures of LiCl and AlCl$_3$) are for one temperature only, 298.15 K (37, 45). The concentration range of this data is 0.000313 M to 2.0 M. The dependence of conductivity on temperature and concentration for concentrations above 2.0 M was estimated from conductivity data for a similar electrolyte, SOCl$_2$ containing SO$_2$, S, and equimolar amounts of LiCl and AlCl$_3$ (46-47). Equation [79] predicts continuous conductivities and derivatives (with respect to concentration and temperature) unlike a conductivity expression presented earlier (7).

No data exists to perform a similar analysis for the diffusion coefficient. The diffusivity was assumed to be a function of temperature and independent of concentration. The dependence of diffusivity on temperature was assumed to be identical to the dependence of conductivity on temperature as was done in previous work (7). The expression used here is

$$D = \beta_6 \exp(\beta_4/T) \qquad [80]$$

where $\beta_6 = 1.0 \times 10^{-4}\ cm^2/s$.

LIST OF SYMBOLS

a	specific active surface area of the porous material, cm^{-1}
a^o	initial value of a, cm^{-1}
a^θ	property expressing secondary reference state of electrolyte, cm^3/mol
c	concentration of the electrolyte, mol/cm^3
c_i	concentration of species i, mol/cm^3
$c_{i,ref}$	reference concentration of species i, mol/cm^3
C	heat capacity of the cell, $J/cm^2 K$
D	diffusion coefficient of the binary electrolyte. cm^2/s
D_{eff}	effective diffusion coefficient of electrolyte, cm^2/s
E	cell voltage, V
E_{oc}	open-circuit voltage of the cell, V
E_{tn}	thermoneutral potential of the cell, V
exf	exponent for calculating effective properties in the LiCl film
$expe$	exponent for calculating effective properties in the porous electrode region
exs	exponent for calculating effective properties in the separator
f	mean activity coefficient of electrolyte
F	Faraday's constant, $96487\ C/mol\ of\ electrons$
h_o	heat transfer coefficient, $W/cm^2 K$
i_k	reaction rate of electrochemical reaction k, A/cm^2
$i_{o,k,ref}$	exchange current density of reaction k at c_{ref}, A/cm^2
i_1	superficial current density in the matrix phase, A/cm^2
i_2	superficial current density in the solution phase, A/cm^2
I	total cell current density, A/cm^2
j	current transferred between phases, A/cm^3
$K_{i,l}$	friction coefficient for interaction between species i and l, Js/cm^5
mp	morphology parameter
n_k	number of electrons transferred in the electrochemical reaction k
$\mathbf{N}_i$	superficial flux of species i, $mol/cm^2 s$
$p_{i,k}$	anodic reaction order of species i in reaction k
$q_{i,k}$	cathodic reaction order of species i in reaction k
q	net heat in cell, J/cm^3
$\dot{q}_{ht}$	energy change due to heat transfer between cell and surroundings, W/cm^2
$\dot{q}_p$	heat generated due to cell polarization, W/cm^2
$\dot{q}_s$	heat generated due to entropy effects, W/cm^2
R	universal gas constant, $8.3143\ J/mol K$
R_i	production rate of species i due to reaction, $mol/cm^3 s$
S_l	thickness of region l, cm
$s_{i,k}$	stoichiometric coefficient of species i in reaction k

t	time, s
$t_i^{\blacksquare}$	transference number of species i relative to $\mathbf{v}^{\blacksquare}$
T	cell temperature, K
T_A	ambient temperature, K
u	internal energy of the cell, J/cm^3
$U_{k,ref}$	Potential of reaction k relative to the reference electrode, V
$\mathbf{v}_i$	superficial velocity of species i, cm/s
$\mathbf{v}^{\blacksquare}$	superficial volume average velocity, cm/s
$\tilde{V}_i$	partial molar volume of species i, cm^3/mol
w	net work done by or on the cell, J/cm^3
x	normal direction from SEI surface to porous electrode, cm
z_i	charge number of species i

Greek Symbols

$\alpha_{a,k}$	transfer coefficient in the anodic direction of reaction k
$\alpha_{c,k}$	transfer coefficient in the cathodic direction of reaction k
ϵ	porosity or void volume fraction of the porous electrode
ϵ^o	initial porosity of the porous electrode
κ	conductivity of the solution, $\Omega^{-1}cm^{-1}$
κ_{eff}	effective electrolyte conductivity, $\Omega^{-1}cm^{-1}$
μ_i	chemical potential of species i, J/mol
ν_+	number of cations produce by dissociation of electrolyte
ν_-	number of anions produce by dissociation of electrolyte
ν	total number of ions into which one molecule of the salt dissociates
σ	conductivity of the solid, Ω/cm
σ_{eff}	effective conductivity of the matrix phase, Ω/cm
Φ_1	potential in the matrix phase, V
Φ_2	potential in the electrolyte, V

Subscripts

e	electrolyte
f	LiCl film
i	species i
$init$	initial value
k	reaction k
o	solvent
pe	porous electrode
r	reservoir
s	separator
$+$	cation
$-$	anion
1	solid matrix phase
2	electrolyte phase

REFERENCES

1. D. H. Johnson, A. D. Ayers, R. L. Zupancic, V. S. Alberto, and J. C. Bailey, *J. Power Sources*, **12**, 61 (1984).

2. S. Surampudi, G. Halpert, and I Stein, "Safety Considerations of Lithium-Thionyl Chloride Cells," JPL publication 86-15 (June 1986).

3. K. C. Tsaur and R. Pollard, *J. Electrochem. Soc.*, **133**, 2296 (1986).

4. J. R. Driscoll, G. L. Holleck, and D. E. Toland, Proceedings of the 27th Power Sources Symposium, **28**, (1976).

5. G. Halpert, Jet Propulsion Laboratory, personal communication.

6. S. Szpak and H. V. Venkatasetty, *Power Sources 9: Research and Development in Non-Mechanical Electrical Power Sources*, Proceedings of the 13th International Power Sources Symposium held at Brighton, Sept. 1982, J. Thompson, Ed., Academic Press, London, England, 403 (1983).

7. K. C. Tsaur and R. Pollard, *J. Electrochem. Soc.*, **131**, 975 (1984).

8. K. C. Tsaur and R. Pollard, *J. Electrochem. Soc.*, **131**, 984 (1984).

9. K. C. Tsaur, "Analysis of Electrochemical Systems with Multiple Reactions," Ph.D. dissertation, University of Houston, Houston, TX, (1984).

10. L. A. Parnell and S. Szpak, *Electrochimica Acta*, **30**, 913 (1985).

11. S. Szpak, C. J. Gabriel, and J. R. Driscoll, *Electrochimica Acta*, **32**, 239 (1987).

12. Y. I. Cho and G. Halpert, "Heat Dissipation of High Rate Li-SOCl$_2$ Primary Cells," *J. Power Sources* (1986).

13. Y. I. Cho and G. Halpert, "Thermal Analysis of Prismatic Li-SOCl$_2$ Primary Cells," presented at the 32nd International Power Series Symposium, Cherry Hill, NJ (May, 1986).

14. Y. I. Cho, *J. Electrochem. Soc.*, **134**, 771 (1987).

15. H. Gu, T. V. Nguyen, and R. E. White, "A Mathematical Model for the Lead-Acid Cell: Discharge, Rest, and Charge," in press.

16. W. H. Tiedemann and J. Newman, *Proceedings of the Symposium on Battery Design and Optimization*, S. Gross, Ed., The Electrochemical Society, Inc., Princeton, NJ, Proceedings Volume 79-1, 23 (1979).

17. E. C. Dimpault-Darcy, T. V. Nguyen, and R. E. White, "A Two Dimensional Mathematical Model of a Porous Lead Dioxide Electrode in a Lead-Acid Cell," in press.

18. R. Pollard and J. Newman, *J. Electrochem. Soc*, **128**, 491 (1981).

19. R. Pollard and J. Newman, *J. Electrochem. Soc.*, **128**, 503 (1981).

20. J. Newman and W. Tiedemann, *AIChE. J.*, **21**, 25 (1975).

21. J. A. Trainham, "Flow-Through Porous Electrodes," Ph.D. Dissertation, University of California, Berkeley, CA, (1979).

22. K. Nisancioglu, "Diffusion in Concentrated Electrolyte Solutions," M.S. Thesis, University of California, Berkeley, CA, (1970).

23. J. Newman, D. Bennion, and C. W. Tobias, *Ber. Bunsenges. Phys. Chem.*, **69**, 608 (1965).

24. J. S. Newman, "Electrochemical System," Prentice Hall, Inc., Englewood Cliffs, NJ (1971).

25. R. W. Watts, "A Mathematical Model of the NASA Redox Flow Cell," M. S. Thesis, North Carolina State University, NC, (1983).

26. S. Whitaker, *Chemical Engineering Education*, 18 (Winter 1985).

27. J. S. Dunning, Ph.D. Dissertation, University of California, Los Angelos, CA (1971).

28. R. B. Bird, W. E. Stewart, and E. N. Lightfoot, "Transport Phenomena," John Wiley & Sons, Inc., NY, (1960).

29. K. Denbigh, "The Principles of Chemical Equilibrium," Fourth Ed., Cambridge University Press, London, England, (1981).

30. R. E. White, S. E. Lorimer, and R. Darby, *J. Electrochem. Soc.*, **130**, 1123 (1983).

31. J. S. Dunning, D. N. Bennion, and J. Newman, *J. Electrochem. Soc.*, **120**, 906 (1973).

32. A. N. Dey, *Thin Solid Films*, **43**, 131 (1977).

33. A. N. Dey, *Electrochimica Acta.*, **21**, 377 (1976).

34. R. V. Moshtev, Y. Geronov, and B. Puresheva, *J. Electrochem. Soc.*, **128**, 1851 (1981).

35. E. Peled, *J. Power Sources*, **9**, 253 (1983).

36. N. A. Godshall and J. R. Driscoll, *J. Electrochem. Soc.*, **131**, 2221 (1984).

37. J. J. Auborn, K. W. French, S. I. Lieberman, V. K. Shah, and A. Heller, *J. Electrochem. Soc.*, **120**, 1613 (1973).

38. W. K. Behl, J. A. Christopulos, M. Ramirez, and S. Gilman, *J. Electrochem. Soc.*, **120**, 1619 (1973).

39. K. M. Abraham, L. Pitts, and W. P. Kilroy, *J. Electrochem. Soc.*, **132**, 2301 (1985).

40. K. A. Klinedinst and M. J. Domeniconi, *J. Electrochem. Soc.*, **127**, 539 (1980).

41. K. A. Klinedinst, *J. Electrochem. Soc.*, **132**, 2044 (1985).

42. R. E. White, *Ind. Eng. Chem. Fundam.*, **17**, 367 (1978).

43. C. deBoor, "A Practical Guide to Splines," Springer-Verlag New York Inc., New York, NY (1978).

44. T. I. Evans and R. E. White, *J. Electrochem. Soc.*, submitted for publication.

45. H. V. Venkatasetty and D. J. Saathoff, *J. Electrochem. Soc.*, **128**, 773 (1981).

46. S. Szpak and H. V. Venkatasetty, *J. Electrochem. Soc.*, **131**, 961 (1984).

47. NOSC Tech. Note 1083, S. J. Szpak, Ed., (Nov. 1978).

48. S. Szpak and J. R. Driscoll, *J. Power Sources*, **10**, 343 (1983).

49. R. H. Perry and C. H. Chilton, "Chemical Engineers' Handbook," 5th ed., McGraw-Hill, New York (1973).

50. A. N. Dey, *J. Electrochem. Soc.*, **126**, 2052 (1979).

Table I. Parameter values used in model

Physical properties

Parameter	Value	Ref.	Parameter	Value	Ref.
ν_+	1		ν_-	1	
z_+	1		z_-	-1	
$t_+^{\blacksquare}$	0.5		$t_-^{\blacksquare}$	0.5	
$\tilde{V}_e$ (cm^3/mol)	77.97	7, 38	$\tilde{V}_o$ (cm^3/mol)	72.63	46
$\tilde{V}_{LiCl}$ (cm^3/mol)	20.5	49	σ $(\Omega^{-1}cm^{-1})$	45.5	50
D (cm^2/s)	†		κ $(\Omega^{-1}cm^{-1})$	†	
E_{tn} (V)	-3.723	36	dE/dT (V/K)	$2.28\text{x}10^{-4}$	36
C (J/cm^2K)	0.2	5, 7, 14			

Kinetic parameters

Li oxidation (reaction 1)			SOCl$_2$ reduction (reaction 4)		
Parameter	Value	Ref.	Parameter	Value	Ref.
$s_{+,1}$	-1		$s_{-,4}$	-2	
			$s_{o,4}$	-1	
			$s_{LiCl,4}$	2	
$q_{+,1}$	1		$q_{+,4}$	1	
			$q_{o,4}$	0.5	
$i_{o,1,ref}$ (A/cm^2)	$5.0\text{x}10^{-4}$		$a^o i_{o,4,ref}$ (A/cm^3)	1.0	
			mp	0.05	31
$U_{1,ref}$ (V)	$E_{tn} + T\frac{dE}{dT}$	36	$U_{4,ref}$ (V)	0.0	
$\alpha_{a,1}$	0.25		$\alpha_{a,4}$	1	
$\alpha_{c,1}$	0.75		$\alpha_{c,4}$	1	
n_1	1		n_4	2	

† see appendix

Table II. Base case values of the independent adjustable parameters

Parameter	Value	Parameter	Value
S_{pe} (cm)	0.0335	ϵ^o	0.85
S_r (cm)	0.01		
S_s (cm)	0.0127	ϵ_s	0.7
S_f (cm)	0.001	ϵ_f	0.1
c_{init} (M)	1.5	h_o $(J/cm^2 Ks)$	$6.0\mathrm{x}10^{-4}$
I (A/cm^2)	0.03	T_A (K)	298.15

LIST OF FIGURE CAPTIONS
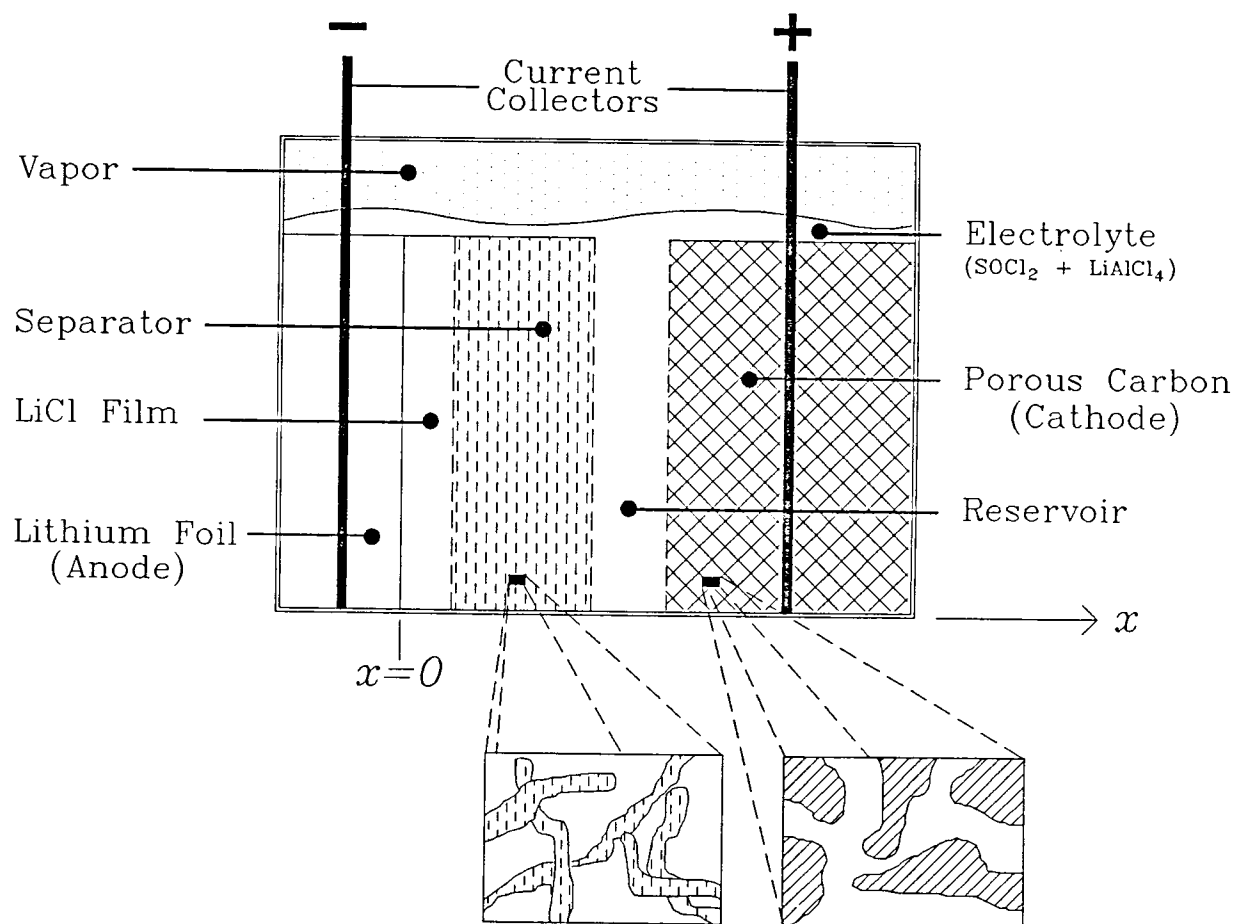
Figure 1. Evans, Nguyen, and White
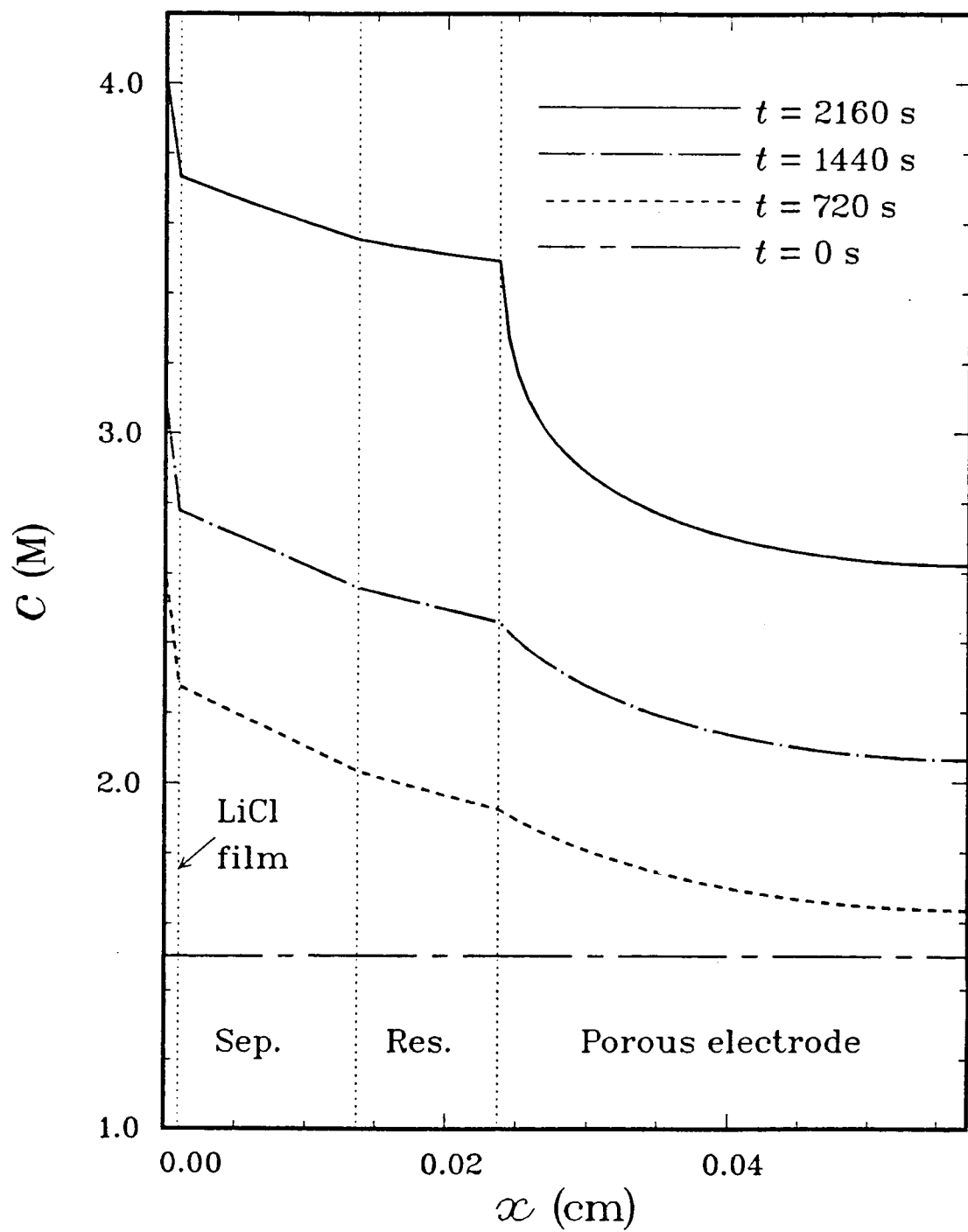
Figure 2. Evans, Nguyen, and White
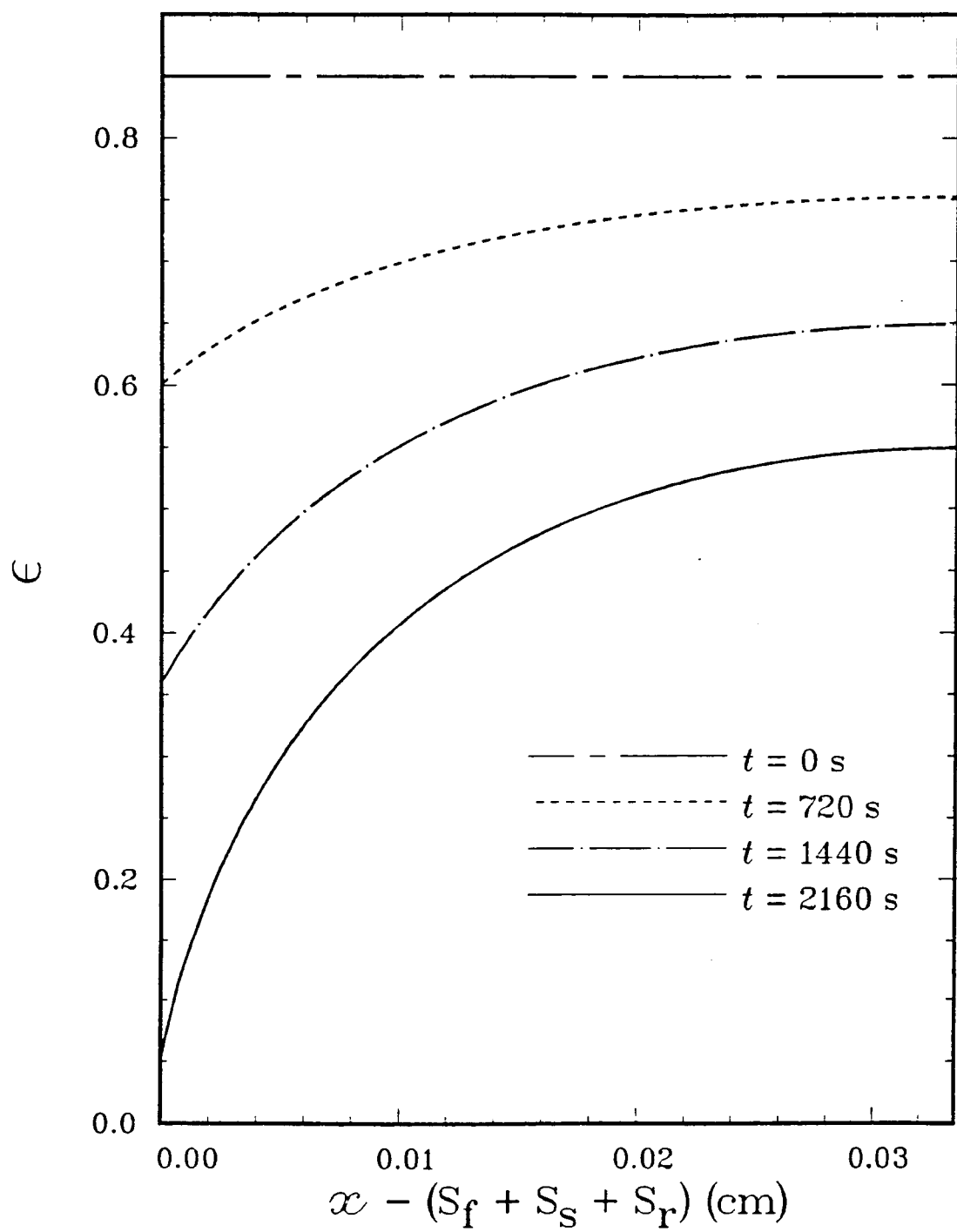
Figure 3.   Evans, Nguyen, and White
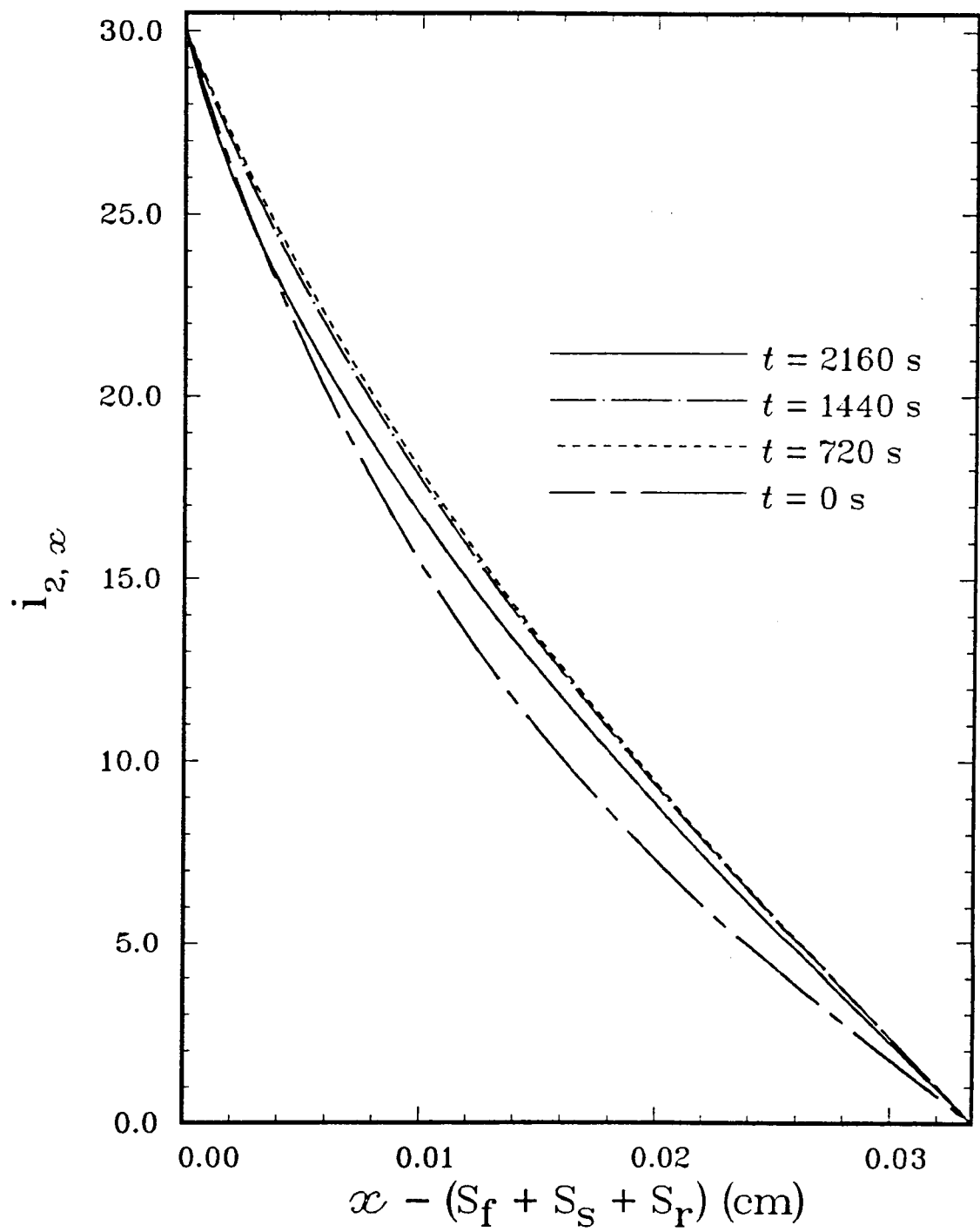
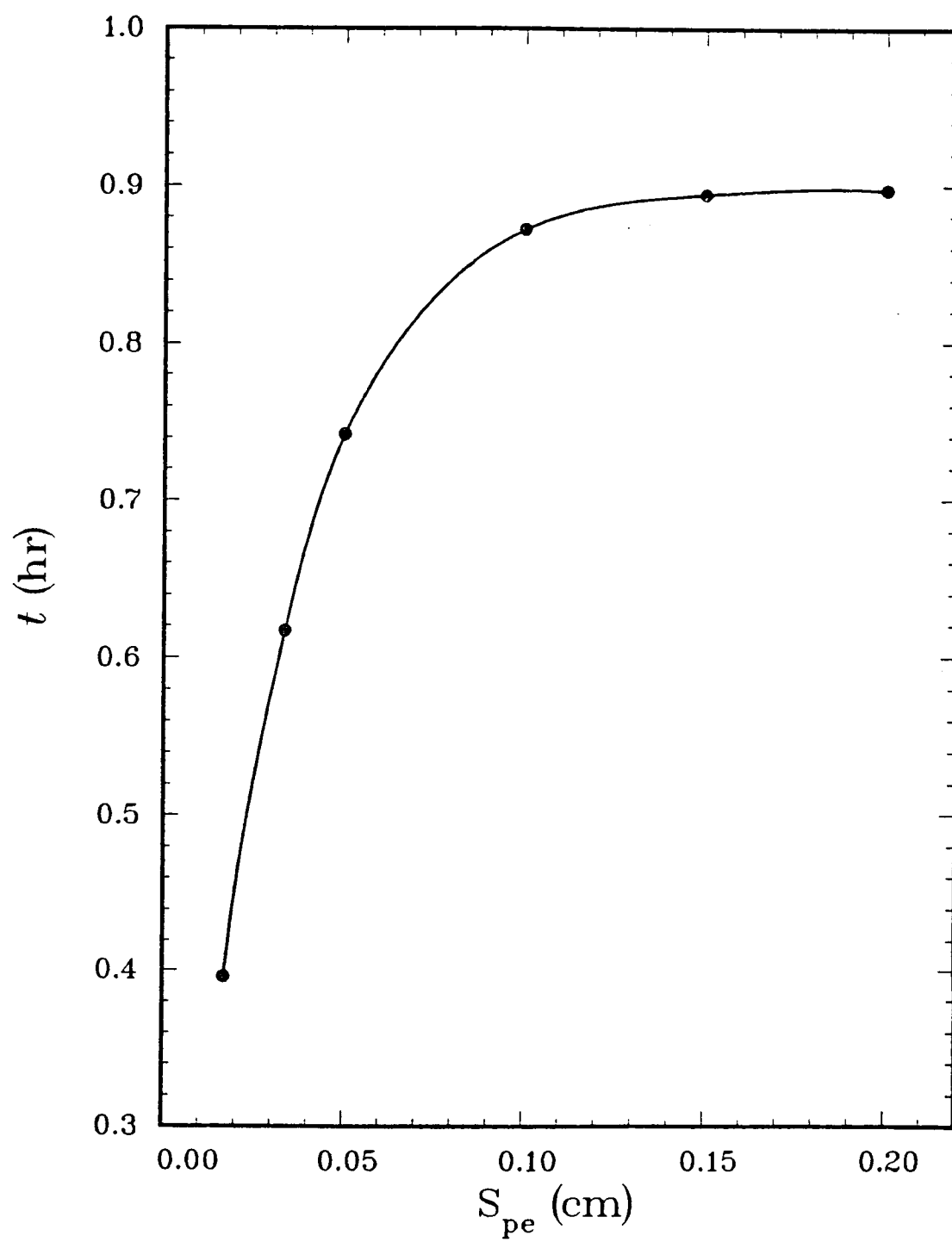Figure 4. Evans, Nguyen, and White
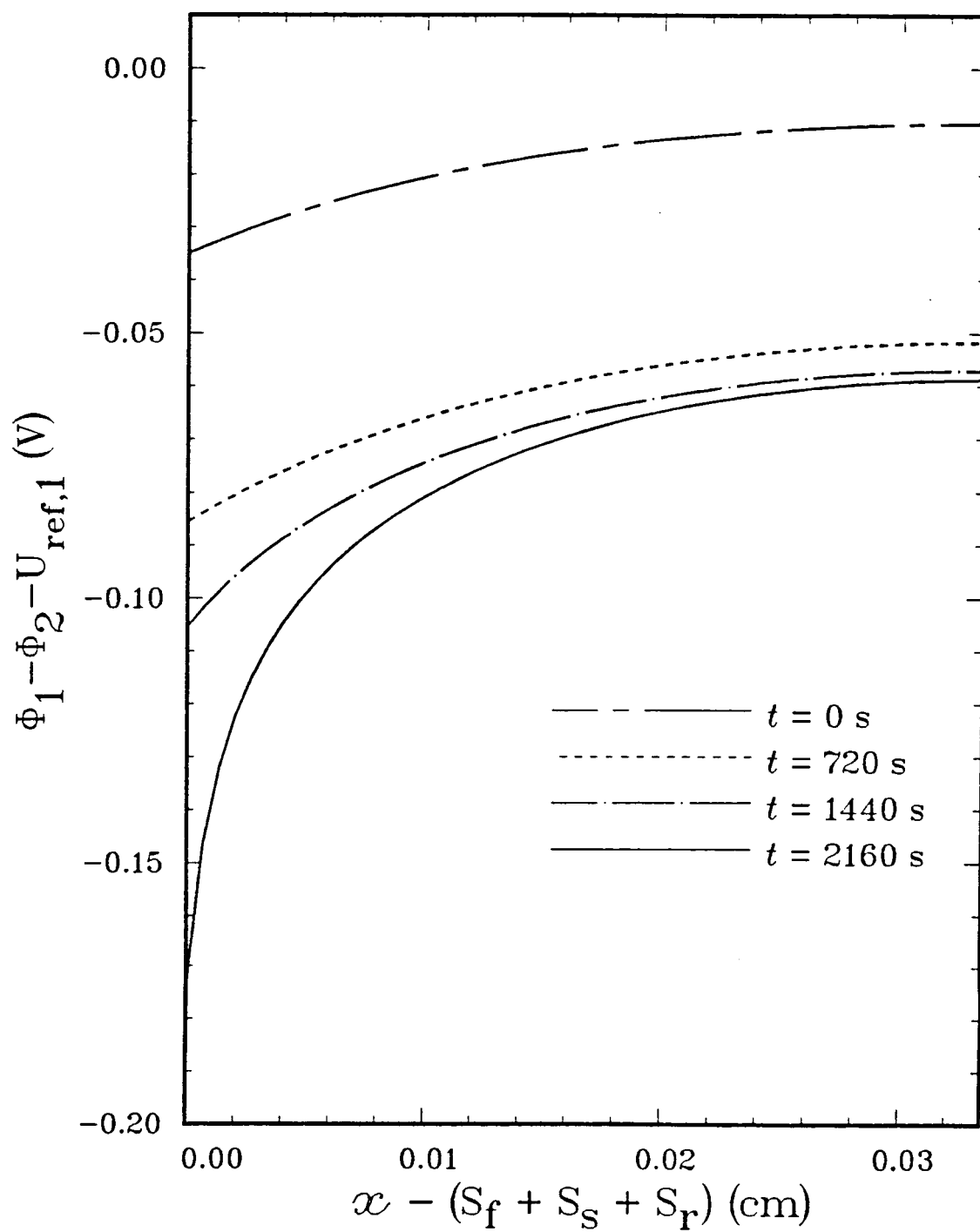
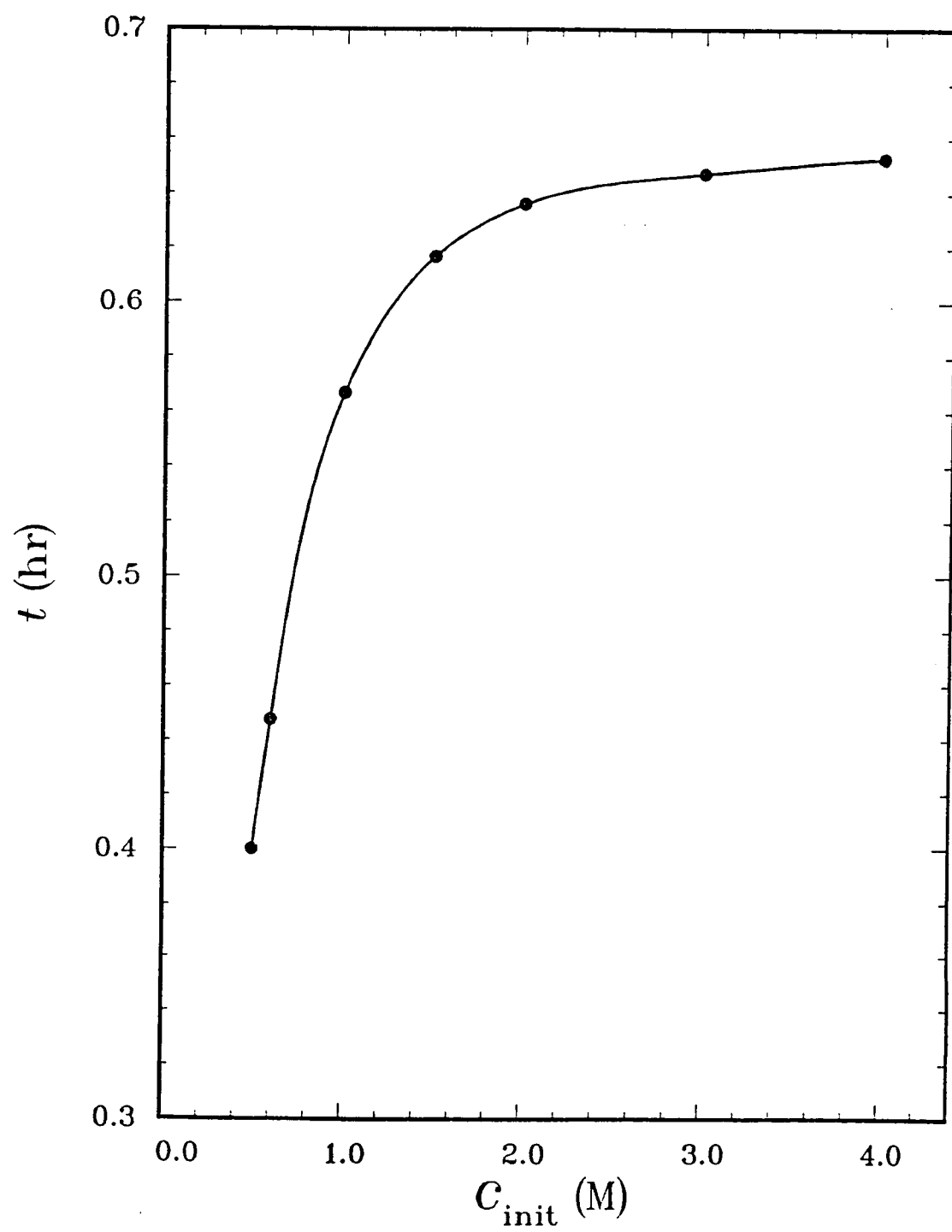Figure 5.   Evans, Nguyen, and White

Figure 6. Evans, Nguyen, and White

Figure 7.   Evans, Nguyen, and White
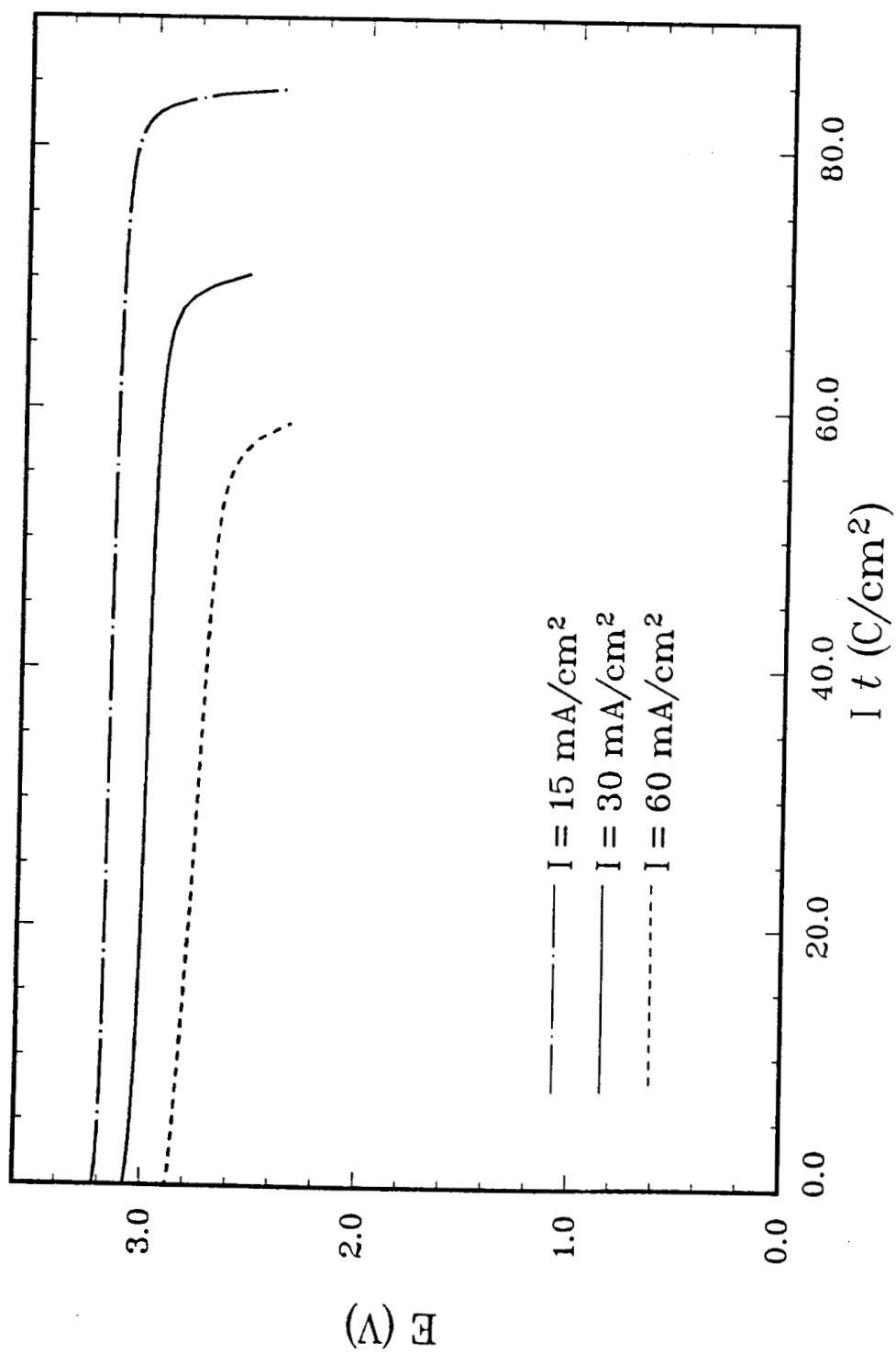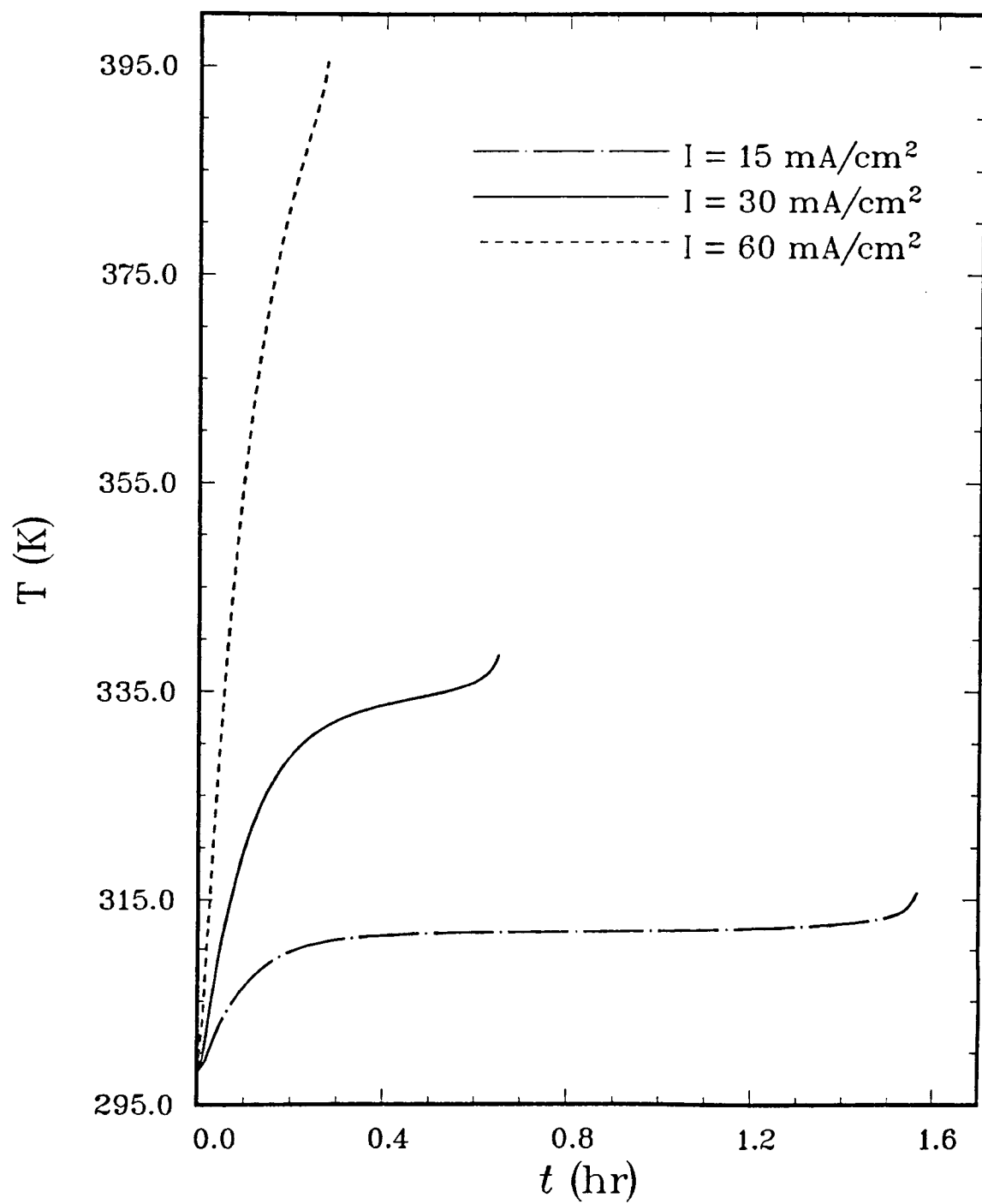
Figure 8. Evans, Nguyen, and White

Figure 9.   Evans, Nguyen, and White